than double that of Pt-Ru under short circuit conditions. This difference is especially striking when one considers that the Pt-Ru, prepared by a proprietary method, is an optimized, high-surface-area catalyst [measured Brunauer–Emmet–Teller (BET) surface area of 65 m^2/g]. The quaternary catalyst, made by borohydride reduction, is not optimized and has roughly half (31 m^2/g) the surface area. This difference indicates that the intrinsic activity of Pt-Ru-Os-Ir per surface atom is several times greater than that of Pt-Ru. Why the addition of relatively small amounts of Os and Ir causes such a substantial increase in activity is an interesting question, to which we currently have no answer.

This study illustrates some of the strengths of the combinatorial method as applied to catalysis. It is possible to search a fairly large phase space rapidly and exhaustively. Although the best catalyst is close in composition to previously known binaries and ternaries, it is markedly superior in performance. Although this catalyst might have been looked for by extrapolation of the binary and ternary results, a serial search of this composition space would be very time-consuming. Further, the combinatorial approach identifies active compositions in regions bounded by inactive binaries—that is, where a targeted, serial search would not normally be done. Finally, we note that the optical screening method developed for anode catalysts might be applied to various electrochemical materials problems (electrocatalysis, battery materials, corrosion) by using the appropriate fluorescent chemosensor molecules.

REFERENCES AND NOTES

1. S. P. Fodor *et al.*, *Science* **251**, 767 (1991).
2. K. S. Lam *et al.*, *Nature* **354**, 82 (1991).
3. R. A. Houghten *et al.*, *ibid.*, p. 84.
4. L. C. Bock, L. C. Griffin, J. A. Latham, E. H. Vermann, J. J. Toole, *ibid.* **355**, 564 (1992).
5. C. Y. Cho *et al.*, *Science* **261**, 1303 (1993).
6. B. L. Bunin and J. A. Ellman, *J. Am. Chem. Soc.* **114**, 10997 (1992).
7. A. A. Virgilio and J. A. Ellman, *ibid.* **116**, 11580 (1994).
8. S. H. DeWitt *et al.*, *Proc. Natl. Acad. Sci. U.S.A.* **90**, 6909 (1993).
9. D. A. Campbell, J. C. Bermak, T. S. Burkoth, D. V. Patel, *J. Am. Chem. Soc.* **117**, 5381 (1995).
10. M. H. Ohlmeyer *et al.*, *Proc. Natl. Acad. Sci. U.S.A.* **90**, 10922 (1993).
11. M. Torneiro and W. C. Still, *J. Am. Chem. Soc.* **117**, 5887 (1995).
12. J. J. Hanak, *J. Math. Sci.* **5**, 964 (1970).
13. E. Danielson *et al.*, *Science* **279**, 837 (1998).
14. R. B. van Dover, L. F. Schneemeyer, R. M. Fleming, *Nature* **392**, 162 (1998).
15. T. A. Dickinson, D. R. Walt, J. White, J. S. Kauer, *Anal. Chem.* **69**, 3413 (1997).
16. G. Briceño, H. Chang, X. Sun, P. G. Schultz, X.-D. Xiang, *Science* **270**, 273 (1995).
17. X.-D. Xiang *et al.*, *ibid.* **268**, 1738 (1995).
18. F. C. Moates *et al.*, *Ind. Eng. Chem. Res.* **35**, 4801 (1996).
19. S. J. Taylor and J. P. Morken, *Science* **280**, 267 (1998).
20. T. F. Fuller, *Electrochem. Soc. Interface* **1997**, 26 (1997).
21. M. Watanabe, M. Vehida, S. Motoo, *J. Electroanal. Chem.* **229**, 395 (1987).
22. K. L. Ley *et al.*, *J. Electrochem. Soc.* **144**, 1543 (1997).
23. R. Parsons and T. Vandernoot, *J. Electroanal. Chem.* **257**, 9 (1988).
24. T. Frelink, W. Vissher, A. P. Cox, J. A. R. van Veen, *Electrochim. Acta* **40**, 1537 (1995).
25. H. Mori *et al.*, *Chem. Pharm. Bull.* **41**, 1944 (1993).
26. A. V. Lemmo, J. T. Fisher, H. M. Geysen, D. J. Rose, *Anal. Chem.* **69**, 543 (1997).
27. A. P. Blanchard, R. J. Kaiser, L. E. Hood, *Biosens. Bioelectronics* **11**, 687 (1996).
28. D. W. McKee, *J. Catal.* **14**, 355 (1969).
29. Metal salts were printed with an Apple Color Stylewriter 2500 onto Toray carbon rectangles taped to ordinary paper. The pattern for each element was drawn in gray scale with commercial drawing software. The printer was calibrated by ultraviolet-visible spectroscopy by printing a highly absorbing organic dye onto transparencies and then desorbing each spot into a known volume of solution. The reduction step was carried out by clamping the array into a home-built Plexiglas device that provided solution wells in the quaternary or five-pick-four pattern. In each well, the printed metal salts were redissolved in a buffered solution (2 μl of 2 M $NaHCO_3$) and then reduced (1 μl of 5% $NaBH_4$).
30. The aqueous indicator solution was 6 M methanol, 0.5 M $NaClO_4$, 30 mM $Ni(ClO_4)_2$, and 100 μM PTP adjusted to pH 3 with $HClO_4$. The carbon substrate has a small resistance (1 to 3 ohms), which translates to a negligible potential drop at the screening currents used (about 1 mA). Bulk samples of catalysts were prepared by dissolving the appropriate metal salts in water to attain an overall concentration of 2 mM. The pH was adjusted to 9, and a 10-fold excess of 5 weight % sodium borohydride was added at one drop per minute. The black precipitate was washed 10 times with water and dried at 110°C. Fuel cell membrane-electrode assemblies were constructed from Nafion 117 by preparing a suspension of the catalyst in 15 weight % soluble Nafion and painting the material onto a decal as described in detail in (*22*).
31. We thank A. Czarnik, D. L. Feldheim, R. Wodd, X.-D. Xiang, and P. G. Schultz for helpful discussions; Todd LaFrenz for performing BET measurements; and the Office of Naval Research (LBL Molecular Design Institute), the Defense Advanced Research Projects Agency, and the Army Research Office for financial support.

16 March 1998; accepted 6 May 1998

Compatibility of Rhenium in Garnet During Mantle Melting and Magma Genesis

Kevin Righter* and Erik H. Hauri

Measurements of the partitioning of rhenium (Re) between garnet and silicate liquid from 1.5 to 2.0 gigapascals and 1250° to 1350°C show that Re is compatible in garnet. Oceanic island basalts (OIBs) have lower Re contents than mid-ocean ridge basalt, because garnet-bearing residues of deeper OIB melting will retain Re. Deep-mantle garnetite or eclogite may harbor the missing Re identified in crust-mantle mass balance calculations. Oceanic crust recycled into the upper mantle at subduction zones will retain high Re/Os (osmium) ratios and become enriched in radiogenic ^{187}Os. Recycled eclogite in a mantle source should be easily traced using Re abundances and Os isotopes.

The Re-Os isotopic system provides constraints on the role of crustal recycling into Earth's deep interior (*1*). Both elements exhibit siderophile behavior in metal-silicate systems, yet in mantle and crustal melting environments, Re is thought to be strongly incompatible (partitioned into magma) and Os strongly compatible (partitioned into the residue) (*2*). Several aspects of the geochemical behavior of Re during mantle melting have remained uncertain. First, oceanic island basalts (OIBs) and some picrites have lower Re contents than mid-ocean ridge basalt (MORB) (*3*), but just the opposite is expected for an incompatible element controlled by the extent of partial melting. Second, the mass of Re in the primitive mantle cannot be balanced by the sum of the continental crust and depleted mantle reservoirs (*4*). Finally, oceanic crust with a high Re/Os ratio is injected into the mantle at subduction zones, yet it is not known whether the Re is lost to fluids in the subduction zones or is retained in eclogite and recycled back into the mantle.

Rhenium is incompatible in most silicate phases such as clinopyroxene and olivine (*5*), but its behavior in garnet-bearing systems at depths >100 km in the mantle has been uncertain. Several observations suggest that garnet may play a role in fractionating Re from Os. Garnet separates from a garnet pyroxenite have almost 10 times more Re than the bulk rock (*6*). Data from oceanic basalts show that Re and Yb behave similarly during mantle melting (*3*); and because Yb is compatible in garnet (*7*), a similar behavior has been hypothesized for Re (*3*). Re-Al_2O_3 systematics in orogenic lherzolites also suggest a link between Re and garnet (*8*). In order to better under-

---

K. Righter, Lunar and Planetary Laboratory, University of Arizona, Tucson, AZ 85721, USA.
E. H. Hauri, Department of Terrestrial Magnetism, Carnegie Institution of Washington, Washington, DC 20015, USA.

*To whom correspondence should be addressed. E-mail: righter@lpl.arizona.edu

stand the behavior of Re, we conducted an experimental study of the partitioning of Re between garnet and silicate liquid at pressure, temperature, and redox conditions relevant to the genesis of oceanic basalt.

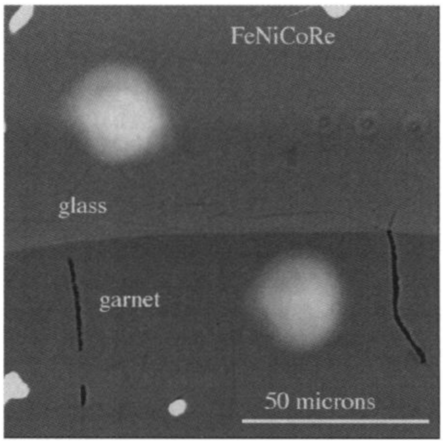

Fig. 1. Backscattered electron image of garnet and silicate melt (quenched to glass) produced in experiment KR-47. The bright circular areas are pits produced during sputtering of the sample by O^- ions. The small size of the ion beam allows metallic flakes to be avoided during analysis and thus avoids the nugget effect that plagues analysis of highly siderophile elements.

We studied a synthetic basalt (Table 1) in the system SiO_2-Al_2O_3-FeO-MgO-CaO; for this composition, garnet and orthopyroxene are liquid phases at ~1.5 to 2.0 GPa and 1250° to 1350°C. Experiments were done in a ½-inch piston cylinder apparatus (*9*); basalt samples were held in either graphite-lined Pt or in FeNiCo alloy capsules. Oxygen fugacities (f_{O_2}) in these capsules are ap proximately 2.5 and 4.5 log f_{O_2} units below the fayalite-magnetite-quartz buffer, which is within the range of terrestrial mantle f_{O_2} (*10*). Run products include pyroxenes, garnet (Fig. 1), Re metal, or FeNiCoRe alloy and silicate melt (quenched to a glass), as well as minor amounts of hercynitic spinel (see Table 1); phases were analyzed by electron microprobe and secondary ion mass spectrometry (*11*, *12*). Evidence for the attainment of equilibrium during the runs was provided by the measured garnet-liquid exchange distribution coefficient, $K_d^{\text{FeO-MgO}}$

$$[(X^{\text{gt}}_{\text{FeO}} \cdot X^{\text{liq}}_{\text{MgO}})/(X^{\text{liq}}_{\text{FeO}} \cdot X^{\text{gt}}_{\text{MgO}})]$$

where X = mole fraction (Table 1) and garnet/liquid partition coefficients [D = (weight % element in garnet)/(weight % element in liquid)] $D^{\text{La, Gd, Yb}}$, which are in agreement with previous work (*13*, *14*).

The data show that Re is compatible in garnet [in an average of four runs, D = 2.7 (Table 1)]; thus, garnet is a host phase for Re during melting of the mantle. Conversely, Re is incompatible in orthopyroxene (Table 1), clinopyroxene, and olivine (*5*). For these partition coefficients, 35 to 95% of the Re in a typical garnet peridotite would be hosted by garnet, depending on how strongly Re partitions into an Fe-Ni sulfide phase (*15*).

Ocean island basalts have lower Re contents than MORB [mean MORB Re = 0.926 parts per billion (ppb) (*2*, *16*, *17*), and mean OIB = 0.377 ppb (*18*, *19*)]. Formation of both types of magmas leaves residual sulfide in the mantle source (*20*), but because partition coefficients for Re between sulfide liquids and silicate liquids are large, Re concentrations in derivative partial melts should be equally buffered and there should be no discernible difference in the average Re contents of OIBs and MORB. If the presence of residual sulfide had any differential leverage on the Re contents of magmas, it might be expected that MORB would have lower Re contents than OIBs, because the lower relative f_{O_2} during MORB genesis (*10*) would favor partitioning of Re into the sulfide. The lower Re contents of OIBs, however, are just the opposite of this expectation, indicating that another phase is involved. Our data

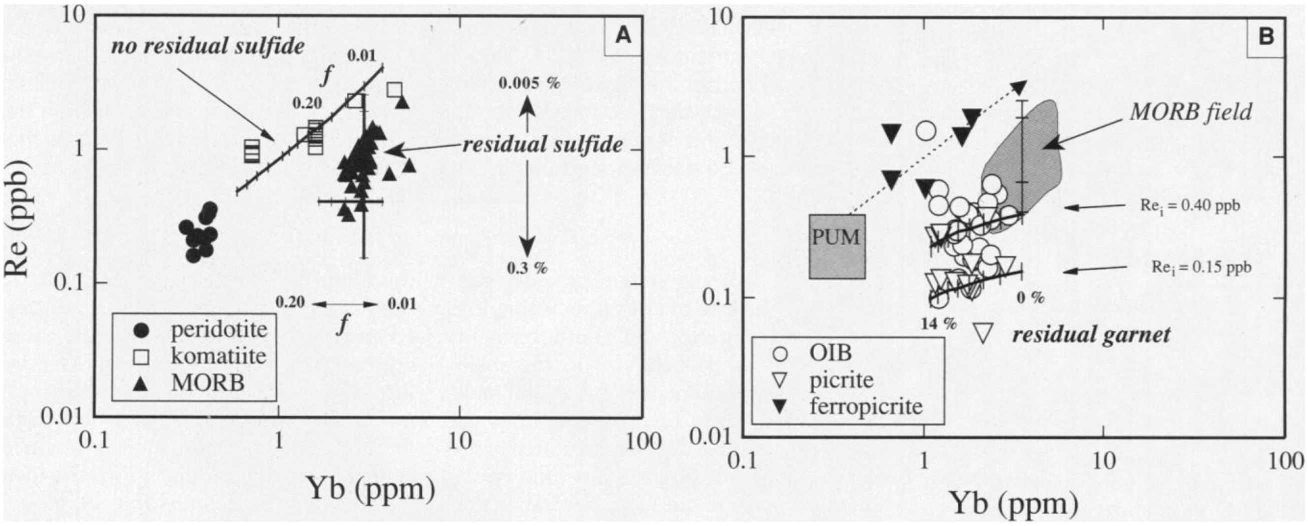

Fig. 2. Mantle melting relations for Re and Yb. (**A**) Melting with no residual garnet. The positive trend for peridotites and komatiites is consistent with the incompatibility of both elements during large degrees of mantle melting, where no sulfide or garnet would be left in the residuum; the diagonal line shows the expected trend during equilibrium melting of peridotite, starting with 0.28 ppb Re and 0.40 parts per million (ppm) Yb. The Re concentrations for MORB that plot below this trend are consistent with the presence of small amounts of sulfide liquid in the residual mantle during melting. The horizontal line represents the variation produced by variable degrees of melting with 0.088% residual sulfide in the mantle—the amount expected from fertile mantle with 300 ppm S (*3*). The vertical line represents the effect of increasing or decreasing the amount of residual sulfide present in the residual mantle for a fixed melt fraction (f) of 0.05. Both of the calculated trends for MORB are for X_{olivine} = 55 to 60% and X_{opx} = 20 to 25%, and X_{cpx} = 20% of the solid mantle, where X is the mole fraction. (**B**) Melting with residual garnet. Many picrites and OIBs have even lower Re contents than MORB (shaded area) and occupy a different area inthe Re-Yb diagram; OIB Re-Yb characteristics can be modeled by equilibrium melting of mantle with residual sulfide (fixed at 0.088%) and garnet (0 to 14%; diagonal lines). The upper trend is for a mantle with 0.40 ppb of Re, and the lower trend is for a mantle with 0.15 ppb of Re; this represents the range of Re contents in fertile mantle (*34*). Most picrites can be produced by melting of a mantle that is sulfide-free but garnet-rich, whereas ferropicrites can be generated by melting of a mantle that is sulfide- and garnet-free. The vertical line is for f = 0.02; the steep diagonal dashed line is the same as the diagonal line in (A). PUM, primitive upper mantle. Both of the shallow diagonal trends are for f of 0.02, X_{olivine} = 55 to 60%, X_{opx} = 20 to 25%, and $X_{\text{cpx}} + X_{\text{garnet}}$ = 20% of the solid mantle. Partitioning data for Re are from (*5*), (*16*), and this study, and for Yb from (*35*). For Re: D(oliv) = 0.01; D(opx) = 0.18; D(cpx) = 0.03; D(garnet) = 2.7; and D(sulf) = 900. For Yb: D(oliv) = 0.03; D(opx) = 0.03; D(cpx) = 0.5; D(garnet) = 3; and D(sulf) = 0. Sources of Re and Yb data are peridotite with $Al_2O_3 > 3.0$; (*34*), MORB (*2*, *17*), komatiite (*27*, *28*), OIBs (*18*, *19*), and picrites (*23*, *24*).

imply that the Re abundances of MORB can be modeled by melting a garnet-free but sulfide-bearing residuum (Fig. 2A), consistent with their low platinum group element (PGE) abundances and subdued garnet rare earth element (REE) signature. Oceanic island basalts can be generated with a garnet- and sulfide-bearing residuum (Fig. 2B). For comparison, komatiites and some basaltic tholeiites with high Re concentrations can be derived by melting with no residual garnet or sulfide in the source (Fig. 2A). In a plot of Re and Yb, these lavas, together with mantle peridotite, form a positive trend with a slope of unity, as expected for two incompatible elements (Fig. 2A).

The low bulk Re concentrations of many picrites have been difficult to explain by the presence of residual sulfide in the mantle source (*21*). Many picrites and komatiites are not sulfide saturated (*20*), as indicated by their high PGE concentrations. Our data imply that many picrites [for example, Karoo (*22*) and Siberia (*23*) (Fig. 2)] can be derived by melting with a garnet-bearing but sulfide-free residuum, consistent with their REE and high PGE abundances. Although isotopic data from the Karoo and Siberia localities are also consistent with the involvement of old, Re-depleted, subcontinental lithospheric mantle, such a source is not available beneath Hawaii, where some of the lowest Re contents have been measured in the Hawaiian Scientific Drilling Project picrite samples (*18*). Ferropicrites from the Pechenga region (*24*), on the other hand, have Re contents as high as those in komatiites but are believed to be sulfide saturated. On the basis of major and trace element data, it appears that garnet was not present in the mantle residuum of these picrites (*24*), and thus the high Re contents of ferropicrites relative to those of more normal picrites may be attributed to the absence of garnet in their melting residuum.

Mass balance calculations (*3*, *4*) indicate that the crustal abundance of Re is too low by a factor of 10 to balance the depletion of Re in the MORB mantle (depleted modern mantle), which suggests that there is an unidentified reservoir of Re (Fig. 3). Some have

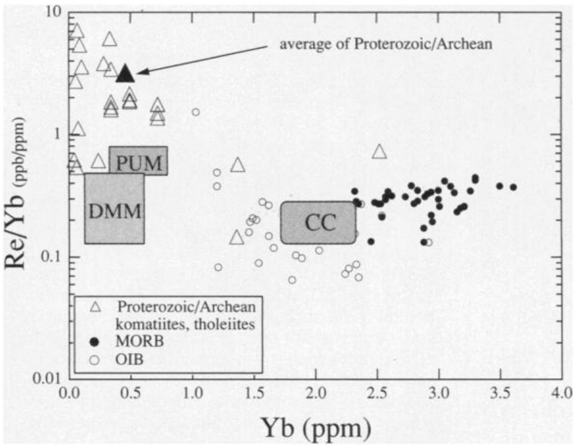

Fig. 3. Re/Yb (ppb/ppm) versus Yb (ppm) for mantle (DMM, depleted modern mantle) and crustal (CC, continental crust) reservoirs (*3*), together with data from Proterozoic/Archean komatiites (*27*), and tholeiites (*27*, *29*). MORB and OIB samples are the same as those presented in Fig. 2.

Table 1. Summary of experimental and analytical results. Starting composition: 50% SiO_2, 13% Al_2O_3, 19% FeO, 11% CaO, and 7% MgO; doped with 5% ReO_2 by weight. Runs 60, 62, and 69 were also seeded with natural Buell Park garnet (*9*). Phase abbreviations are as follows: gl, glass; opx, orthopyroxene; cpx, augite; gt, garnet. ΔFMQ is the f_{O_2} of an experiment relative to the fayalite-magnetite-quartz buffer (*33*).

Run no.	KR-47	Re-60	Re-62	KR-55	Re-69
Duration (hours)	24	48	24	23.5	26
Pressure (GPa)	1.55	1.65	1.85	1.50	2.00
Temperature (°C)	1300	1250	1250	1350	1275
$\log f_{O_2}$ (ΔFMQ)	−10.6 (−4.8)	−8.6 (−2.5)	−8.4 (−2.3)	−10.2 (−4.3)	−8.4 (−2.5)
Phases	gl:opx:gt	gl:opx:sp	gl:opx:cpx:gt	gl:gt:opx	gl:gt:opx:cpx
Proportions (%)	60:20:20	30:60:10	10:40:40:10	50:35:15	40:45:15:5
Phase *n*	Glass 3	Glass 3	Glass 5	Glass 9	Glass 2
SiO_2	45.3 (4)	52.8 (4)	52.1 (3)	43.2 (6)	45.9 (5)
Al_2O_3	11.6 (2)	13.0 (6)	13.1 (2)	9.4 (2)	13.0 (3)
FeO*	28.50 (12)	14.18 (8)	17.92 (15)	32.78 (15)	22.38 (13)
MgO	3.7 (1)	4.1 (1)	3.1 (1)	3.0 (2)	3.7 (1)
CaO	9.29 (6)	9.76 (4)	11.24 (5)	9.68 (4)	10.04 (6)
NiO	ND	ND	0.04 (1)	ND	0.96 (3)
CoO	0.23 (2)	0.25 (1)	0.02 (1)	0.26 (2)	ND
Re (ppm)	1.2 ± 0.8	130 ± 2	24 ± 4	4.7 ± 1.4	11.3 ± 1.5
Mg no.	0.21	0.33	0.23	0.14	0.23
Total*	98.61	94.10	97.45	98.40	96.02
Phase *n*	Garnet 10	Opx 8	Garnet 6	Garnet 10	Garnet 10
SiO_2	38.2 (3)	51.6 (6)	39.3 (2)	38.1 (3)	38.7 (2)
Al_2O_3	21.4 (4)	3.7 (1)	21.1 (4)	21.5 (4)	21.9 (4)
FeO*	26.60 (6)	22.83 (12)	24.87 (11)	27.24 (10)	25.90 (11)
MgO	6.6 (1)	20.5 (3)	7.6 (1)	5.5 (1)	7.5 (1)
CaO	6.98 (6)	2.03 (3)	8.61 (4)	8.21 (4)	6.76 (3)
Re (ppm)	3.6 ± 1.1	26 ± 3	115 ± 25	6.5 ± 1.8	16.2 ± 1.8
Mg no.	0.31	0.46	0.35	0.26	0.34
Total	100.09	101.27	101.43	100.77	100.79
D^{Re} (xtal/liquid)	3.0 (+9.0, −1.8)	0.18 (+0.04, −0.01)	4.8 (+2.2, −1.6)	1.4 (+1.1, −0.6)	1.4 (+0.4, −0.3)
$K_d^{FeO\text{-}MgO}$ (garnet/liquid)	0.52	–	0.56	0.46	0.59
D^{La} (garnet/liquid)†	0.0037	–	0.0110	0.035	0.16
D^{Gd} (garnet/liquid)	0.035	–	0.077	0.060	0.37
D^{Yb} (garnet/liquid)	8.3	–	2.0	6.2	6.4

*The slightly low totals for glasses 60, 62 and 69 are due to impurities (not reported in the table) introduced by the garnet: Ti, Na, Cr, Ni, and Mn; *n*, number of points analyzed by microprobe; ND, not detected. Units in parentheses represent 2σ of replicate analyses in terms of the least units cited. †DLa, Gd, and Yb (garnet/liquid) are based on the ratio of counts normalized to ^{30}Si.

argued that there may be a large percentage of garnetite in the transition zone (*25*); this layer might have originated by segregation of garnet from a magma ocean and remained stable during mantle convection. Dense silicate melt trapped in the deep mantle after crystallization of an early magma ocean may also be capable of sequestering Re. But the most likely scenario is that continuous subduction of oceanic crust to form eclogite introduces garnet-rich and thus Re-rich material into the mantle where it is stored. This last hypothesis is supported by correlations of Os isotopes with isotopes of Sr, Nd, Pb, and O in OIBs, as well as numerous other trace element and isotopic data that are all consistent with recycling of basaltic crust (*3, 19, 26*). A mass of 2.6×10^{26} grams of oceanic crust, introduced into the mantle over 4.5 billion years, would require only 0.650 ppb of Re to balance the Re depletion of the upper mantle (*4*). This concentration is within the range of Re contents of typical MORB [average = 0.926 ppb (*2, 17*)] and Proterozoic/Archean basaltic rocks [average = 0.848 ppb (*27–29*)]. Subducted Proterozoic and Archean ultramafic volcanic rocks could potentially account for all the missing Re and could balance the low Re/Yb ratios of the depleted mantle and the continental crust, because these rocks have Re/Yb ratios well above the primitive mantle ratio (Fig. 3).

The coupled behavior of Re and Yb in oceanic basalts argues against core-mantle interaction to explain the enriched Os isotope signatures of OIBs compared to MORB. Rhenium, a highly siderophile element, is concentrated in the core, in such a way that addition of even 1 weight % core material to OIB sources (*30*) would result in higher Re and Re/Yb in OIBs than in MORB, which is opposite to what is actually observed (Fig. 2B). Garnet-enriched recycled oceanic crust is a more likely source (*31*). Subducted basaltic crust is introduced into the upper mantle with an initially high Re/Os ratio. Within the stability field of garnet (> 90 to 100 km), Re could be retained during dehydration or melting of the slab, and thus garnet may play a role in preserving the high Re/Os ratio (and, with time, high Os isotope ratio) of slab material during subduction zone processing. Elevated Os isotopes should thus be a sensitive indicator of recycled basaltic material, as indicated by Os isotope data for ancient pyroxenites and eclogites (*6, 8, 28*). The high Os isotopic compositions of OIBs, together with the evidence that Re is compatible in garnet, implies that the sources of mantle plumes contain most of the Re, which has been apparently removed from the upper mantle, and that this Re resides in recycled oceanic crust.

REFERENCES AND NOTES

1. C. J. Allegre and J.-M. Luck, *Earth Planet. Sci. Lett.* **48**, 148 (1980).
2. J. W. Morgan and J. F. Lovering, *ibid.* **3**, 219 (1967); J. Hertogen, M.-J. Janssens, H. Palme, *Geochim. Cosmochim. Acta* **44**, 2125 (1980); J. Birck and C. J. Allegre, *Earth Planet. Sci. Lett.* **124**, 139 (1994).
3. E. H. Hauri and S. R. Hart, *Chem. Geol.* **139**, 185 (1997).
4. C. E. Martin, B. K. Esser, K. K. Turekian, *Aust. J. Earth Sci.* **38**, 569 (1991).
5. K. Righter, C. J. Capobianco, M. J. Drake, *Eos* **76**, F698 (1995); E. B. Watson, D. Ben Othman, J.-M. Luck, A. Hofmann, *Chem. Geol.* **62**, 191 (1987).
6. M. Roy-Barman, J.-M. Luck, C. J. Allegre, *Chem. Geol.* **130**, 55 (1996).
7. I. A. Nicholls and K. L. Harris, *Geochim. Cosmochim. Acta* **44**, 287 (1980).
8. L. C. Reisberg, C. J. Allegre, J.-M. Luck, *Earth Planet. Sci. Lett.* **105**, 196 (1991); N. Kumar, L. Reisberg, A. Zindler, *Geochim. Cosmochim. Acta* **60**, 1429 (1996).
9. Synthetic basalt was prepared from oxide powders. Barium carbonate pressure media were used in the piston cylinder assemblies; pressure was calibrated against the melting points of diopside, gold, and nickel (*32*). Temperature was imposed by graphite heaters and controlled with a Type C (W_3Re-$W_{26}Re$) thermocouple. Pyroxene thermometry (in the CaO-MgO-Al_2O_3-SiO_2 system) runs under the same pressure and temperature conditions show that the hot spot is isothermal within 5° to 10°C 3 mm above the thermocouple—the sample/sensor assembly is well within these spatial constraints. For experiments in graphite-lined Pt capsules, f_{O_2} has been monitored with a Co/CoO-MgO redox sensor [J. R. Taylor, V. J. Wall, M. I. Pownceby, *Am. Mineral.* **77**, 284 (1992)]. For experiments in the alloy capsules, f_{O_2} is calculated from the activities of Fe and FeO in the metal and glass phases, respectively [see (*32*)]. In order to promote the growth of large garnets, runs 62 and 69 were seeded with 10% garnet (Re-free) from Buell Park, Arizona [M. J. O'Hara and E. L. P. Percy, *Am. Mineral.* **51**, 336 (1966)]. Samples were pressurized to the desired run pressure plus 15%, heated at a rate of approximately 40°C/min, and held at the set point temperature for 24 to 48 hours before the power to the furnace was turned off.
10. I. S. E. Carmichael, *Contrib. Mineral. Petrol.* **106**, 129 (1991).
11. Major elements in the crystals and glasses from the experimental run products (Table 1) were analyzed with a CAMECA SX50 electron microprobe at the University of Arizona. Operating conditions for analysis of major elements in crystals and glasses were 15-kV accelerating voltage, 30-nA sample current, 10-s counting times, and a point beam; PAP ϕ-ρ-z correction procedures were used [J. L. Pouchou and F. Pichoir, in *Electron Probe Quantitation*, K. F. J. Heinrich and D. E. Newbury, Eds. (Plenum, New York, 1991), pp. 31–75]. Standards used include diopside (Si, Mg, and Ca), fayalite (Fe), and potassium feldspar (Al). The slightly low totals for glasses 60, 62, and 69 are due to impurities (not reported in the table) introduced by the garnet: Ti, Na, Cr, Ni, and Mn.
12. Trace elements Re, Ba, La, Eu, Gd, Tm, and Yb were analyzed by SIMS on a CAMECA 6f-series ion probe at the Department of Terrestrial Magnetism, Washington, DC. Calibration curves of $^{185}\mathrm{Re}^+/^{30}\mathrm{Si}^+$ and $^{187}\mathrm{Re}^+/^{30}\mathrm{Si}^+$ versus Re were constructed for three Re-bearing basaltic glasses, whose Re contents have been determined by electron microprobe analysis. The validity of the ion probe calibration was confirmed by the excellent agreement between SIMS and INAA analysis of a silicate glass with 1 ppm Re [experiment 40 in K. Righter, D. J. Lindstrom, R. R. Martinez, E. H. Hauri, M. J. Drake, *Lunar Planet. Sci.* **XXIX**, 1546 (1998)]. Ion microprobe analyses were done with a 22-kV primary beam of $^{16}\mathrm{O}^-$ ions focused to a 10- to 15-μm spot. Positive secondary ions accelerated at 10 kV with excess kinetic energies of 70 ± 50 eV were allowed into the mass spectrometer. Each analysis consisted of a 5-min pre-sputter period followed by collection of secondary ion intensities for $^{30}\mathrm{Si}$ (for 3 s), $^{137}\mathrm{Ba}$, $^{139}\mathrm{La}$, $^{153}\mathrm{Eu}$, $^{155}\mathrm{Gd}$, $^{169}\mathrm{Tm}$, $^{171}\mathrm{Yb}$, $^{185}\mathrm{Re}$, and $^{187}\mathrm{Re}$ (all for 10 s) and averaged over five counting cycles. Trace element count rates were normalized to that for $^{30}\mathrm{Si}$; $^{185}\mathrm{Re}^+/^{30}\mathrm{Si}^+$ and $^{187}\mathrm{Re}^+/^{30}\mathrm{Si}^+$ ratios were corrected for interferences from TmO^+ and YbO^+, respectively. Standard deviations based on counting statistics are indicated for each Re measurement in Table 1 and are also included in the calculation of uncertainties for each D(Re) crystal/melt.
13. Compare to garnet-liquid $K_d^{\mathrm{FeO\text{-}MgO}} = 0.54 \pm 6$ from experiments of R. J. Kinzler [*J. Geophys. Res.* **102**, 853 (1997)] across a similar pressure and temperature range.
14. Compare to D^{La} (garnet/melt) = 0.0164 to 0.05, D^{Gd} (garnet/melt) = 0.498, and D^{Yb} (garnet/melt) = 3.88 to 8.7 from three different studies: N. Shimizu and I. Kushiro, *Geophys. Res. Lett.* **2**, 413 (1975); I. A. Nicholls and K. L. Harris, *Geochim. Cosmochim. Acta* **44**, 287 (1980); E. H. Hauri, T. P. Wagner, T. L. Grove, *Chem. Geol.* **117**, 149 (1994).
15. The range of Re is derived from calculations using the average garnet/melt partition coefficient from all four runs (*D* = 2.7), and *D*(Re) sulfide/liquid values of 1200 [J. H. Jones and M. J. Drake, *Nature* **322**, 221 (1986)] and 43 (*16*) as upper and lower limits, respectively. Calculations were for a peridotite with 20% garnet and 0.088% sulfide (the amount required if peridotite contains 300 ppm S).
16. M. Roy-Barman, G. J. Wasserburg, D. A. Papanastassiou, M. Chaussidon, *Earth Planet. Sci. Lett.* **154**, 331 (1998).
17. M. Roy-Barman and C. J. Allegre, *Geochim. Cosmochim. Acta* **53**, 1583 (1994); P. Schiano, J.-L. Birck, C. J. Allegre, *Earth Planet. Sci. Lett.* **150**, 363 (1997).
18. E. H. Hauri, J. L. Lassiter, D. J. DePaolo, *J. Geophys. Res.* **101**, 11701 (1996).
19. E. H. Hauri and S. R. Hart, *Earth Planet. Sci. Lett.* **114**, 353 (1993); L. Reisberg *et al.*, *ibid.* **120**, 149 (1993); F. Marcantonio, A. Zindler, T. Elliot, H. Staudigel, *ibid.* **133**, 397 (1995); C. E. Martin, R. W. Carlson, S. B. Shirey, F. A. Frey, C.-Y. Chen, *ibid.* **128**, 287 (1994); E. Widom and S. B. Shirey, *ibid.* **142**, 451 (1996); J. M. Eiler, K. A. Farley, J. W. Valley, A. W. Hofmann, E. M. Stolper, *ibid.* **144**, 453 (1996).
20. R. R. Keays, *Lithos* **34**, 1 (1995); B. J. Fryer and J. D. Greenough, *Can. J. Earth Sci.* **29**, 2329 (1992).
21. M. Roy-Barman and C. J. Allegre, *Earth Planet. Sci. Lett.* **129**, 145 (1995).
22. R. M. Ellam, R. W. Carlson, S. B. Shirey, *Nature* **359**, 718 (1992); K. G. Cox, A. R. Duncan, J. W. Bristow, S. R. Taylor, A. J. Erlank, *Spec. Publ. Geol. Soc. S. Afr.* **13**, 149 (1984).
23. M. F. Horan, R. J. Walker, V. A. Federenko, G. K. Czamanske, *Geochim. Cosmochim. Acta* **59**, 5159 (1995).
24. R. J. Walker, J. W. Morgan, E. Hanski, V. F. Smolkin, *ibid.* **61**, 3145 (1997); E. Hanski, *Lithos* **34**, 40 (1995).
25. A. E. Ringwood, *Geochim. Cosmochim. Acta* **55**, 2083 (1991).
26. W. F. McDonough, *Philos. Trans. R. Soc. London Ser. A* **335**, 407 (1990); C. G. Chase and P. J. Patchett, *Earth Planet. Sci. Lett.* **91**, 66 (1986); J. Blichert-Toft and F. Albarede, *ibid.* **148**, 243 (1997).
27. T. Meisel, G. G. Biino, T. F Nagler, *ibid.* **60**, 2583 (1996); R. J. Walker, S. B. Shirey, O. Stecher, *Earth Planet. Sci. Lett.* **87**, 1 (1988); R. J. Walker, S. B. Shirey, G. N. Hanson, V. Rajamani, *Geochim. Cosmochim. Acta* **53**, 3005 (1989); J. G. Arth, N. T. Arndt, A. J. Naldrett, *Geology* **5**, 590 (1977); V. Rajamani, K. Shivkumar, G. N. Hanson, S. B. Shirey, *J. Petrol.* **26**, 92 (1985).
28. D. G. Pearson *et al.*, *Nature* **374**, 711 (1995); S. Esperanca, R. W. Carlson, S. B. Shirey, D. Smith, *Geology* **25**, 651 (1997).
29. R. J. Walker, L. M. Echeverria, S. B. Shirey, M. F. Horan, *Contrib. Mineral. Petrol.* **107**, 150 (1991).
30. A. D. Brandon, R. J. Walker, J. W. Morgan, M. D. Norman, H. M. Prichard, *Science* **280**, 1570, 1998.

31. Addition of 1 weight % core material to a mantle source will have no effect on the isotopes of Sr, Nd, Pb, and oxygen, which are well correlated with Os isotopes in most OIBs [for example, Hawaii (*18*, *19*)]. Core-mantle interaction would also buffer the f_{O_2} of OIBs to the iron-wustite buffer, which is three to four orders of magnitude lower than f_{O_2}'s actually measured in OIBs [*Basaltic Volcanism Study Project* (Pergamon Press, New York, 1981)].
32. K. Righter, M. J. Drake, G. Yaxley, *Phys. Earth Planet. Int.* **100**, 115 (1997).
33. J. Myers and H. Eugster, *Contrib. Mineral. Petrol.* **82**, 75 (1983).
34. T. Meisel, R. J. Walker, J. W. Morgan, *Nature* **383**, 517 (1996); H. K. Brueckner *et al.*, *J. Geophys. Res.* **100**, 22283 (1995); L. Reisberg and J.-P. Lorand, *Nature* **376**, 159 (1995); J. W. Morgan, G. A. Wandless, R. K. Petrie, A. J. Irving, *Tectonophysics* **75**, 47 (1981).
35. T. H. Green, *Chem. Geol.* **117**, 1 (1994).
36. We thank C. J. Capobianco, J. Chesley, M. J. Drake, S. Shirey, and P. Warren for discussions; P. Liermann and J. Ganguly for providing samples of Buell Park garnet; and J. Wang for expert assistance with the ion microprobe. This research is supported by NSF grants EAR-9706024 and EAR-9628092.

24 March 1998; accepted 29 April 1998

Integrated Optoelectronic Devices Based on Conjugated Polymers

Henning Sirringhaus,* Nir Tessler, Richard H. Friend*

An all-polymer semiconductor integrated device is demonstrated with a high-mobility conjugated polymer field-effect transistor (FET) driving a polymer light-emitting diode (LED) of similar size. The FET uses regioregular poly(hexylthiophene). Its performance approaches that of inorganic amorphous silicon FETs, with field-effect mobilities of 0.05 to 0.1 square centimeters per volt second and ON-OFF current ratios of >10^6. The high mobility is attributed to the formation of extended polaron states as a result of local self-organization, in contrast to the variable-range hopping of self-localized polarons found in more disordered polymers. The FET-LED device represents a step toward all-polymer optoelectronic integrated circuits such as active-matrix polymer LED displays.

Solution-processible conjugated polymers are among the most promising candidates for a cheap electronic and optoelectronic technology on plastic substrates. Polymer LEDs exceeding peak brightnesses of 10^6 cd m^{-2} (*1*) and high-resolution video polymer LED displays (*2*) have been demonstrated. One of the main obstacles to all-polymer optoelectronic circuits is the lack of a polymer FET with sufficiently high mobility and ON-OFF ratio to achieve reasonable switching speeds in logic circuits (*3*) and to drive polymer LEDs.

Conjugated polymer FETs (*4*) typically show field-effect mobilities of $\mu_{FET} = 10^{-6}$ to 10^{-4} cm^2 V^{-1} s^{-1}, limited by variable-range hopping between disordered polymer chains and ON-OFF current ratios of $<10^4$ (*5*). This is much too low for logic and display applications, and therefore all previous approaches to drive polymer LEDs have used polycrystalline (*2*) or amorphous silicon (a-Si) (*6*) technology. Recently, a polymer FET with a mobility of 0.01 to 0.04 cm^2 V^{-1} s^{-1} and an ON-OFF ratio of 10^2 to 10^4 using regioregular poly(hexylthiophene) (P3HT) was described (*7*). The high mobility is related to structural order in the polymer film induced by the regioregular head-to-tail (HT) coupling of the hexyl side chains. However, a clear understanding of the transport mechanism giving rise to the relatively high mobilities is still lacking.

Here, we report a considerably improved P3HT FET reaching mobilities of 0.05 to 0.1 cm^2 V^{-1} s^{-1} and ON-OFF ratios of $>10^6$, the performance of which starts to rival that of inorganic a-Si FETs and enables us to demonstrate integrated optoelectronic polymer devices. As an example, we have chosen a simple pixel-like configuration in which the FET supplies the current to a polymer LED. This allows us to assess the prospects of active-matrix addressing in all-polymer LED displays.

To construct the multilayer device (Fig. 1A), we first fabricated the FET by spin-coating a film of P3HT (500 to 700 Å) (*8*) onto a highly doped n$^+$-Si wafer with a 2300 Å SiO$_2$ gate oxide (capacitance C_i = 15 nF cm^{-2}). Au source-drain contacts were deposited onto the P3HT through a shadow mask. Then, a layer of SiO$_x$ was thermally evaporated through another, mechanically aligned, shadow mask to define the active LED area on the finger-shaped Au FET drain electrode acting as the hole-injecting anode of the LED. A single layer of poly[2-methoxy-5-(2′-ethyl-hexyloxy)-*p*-phenylene-vinylene] (MEH-PPV) was spin-coated on top. Evaporation of a semitransparent Ca-Ag cathode completed the device. No photolithographic steps were involved. The device

---

Cavendish Laboratory, University of Cambridge, Madingley Road, Cambridge CB3 0HE, UK.

*To whom correspondence should be addressed.

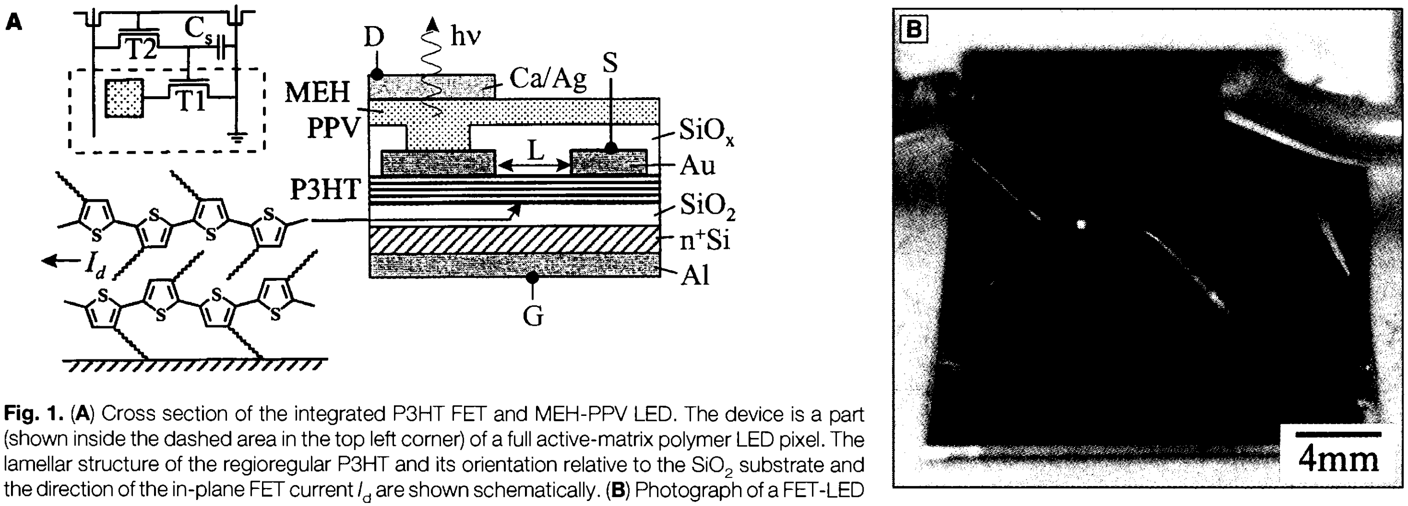

Fig. 1. (**A**) Cross section of the integrated P3HT FET and MEH-PPV LED. The device is a part (shown inside the dashed area in the top left corner) of a full active-matrix polymer LED pixel. The lamellar structure of the regioregular P3HT and its orientation relative to the SiO$_2$ substrate and the direction of the in-plane FET current I_d are shown schematically. (**B**) Photograph of a FET-LED with one of the four "pixels" switched on. The MEH-PPV layer (orange) was made to cover the substrate only partially in order to make the underlying (blueish) P3HT layer visible.